# Response to the comments of Reviewer 2

First of all, we would like to thank the anonymous reviewer for the careful review and valuable suggestions. We carefully revised the manuscript following the suggestions. Hereby we give a point-by-point reply to address the comments. In this document, the words in *italics are the reviewers' comments*, the words in blue are the modifications we have made in the revision, and others are our responses.

**Q1:** *In this interesting paper, a new method for the retrieval of total ice freeboard (ice freeboard plus snow thickness) from single-pass interferometric SAR is developed and applied to the Weddell and Ross Seas. The SAR-derived sea ice topography is validated by independently measured sea ice freeboard profiles and analyzed in comparison to several studies, which support the results. The paper should definitely be published, but I recommend modifications which concern the use of certain terms and the need for additional information. The latter is in particular important for the description of the method.*

**A1:** We thank the reviewer for the positive comment about our research. We have carefully revised the manuscript based on the following comments.

**Q2:** *Line 3: "accurate sea ice DEMs (i.e., snow freeboard)" The term "snow freeboard" (see also line 21 in the introduction) is misleading. Better use "total freeboard" which is ice freeboard plus snow layer thickness*

**A2:** We apologize for any confusion caused by the term "snow freeboard." In this paper, when referring to sea ice DEMs, we actually mean the total freeboard, which includes both the ice freeboard and the thickness of the snow layer. Therefore, whenever we mention "sea ice elevation," it actually means the total freeboard. In the revised version, we have explicitly defined sea ice DEMs as total freeboard (snow+ice). Moreover, we have replaced the old term "sea ice elevation" with "total freeboard" throughout the manuscript, including both the text and figures, to ensure clarity and consistency.

**Q3:** *Lines 21-22: It is the mass of the ice above the water surface plus snow load (not snow freeboard) from which ice thickness can be estimated.*

**A3:** We apologize for the confusing term. The sentence has been revised as: Moreover, the DEM (i.e., total freeboard) can be converted to thickness with the knowledge of snow depth and the assumed values of snow, ice, and seawater densities (Kwok and Kacimi, 2018). Estimating sea ice thickness over time offers valuable insights into the overall stability of sea ice in the changing climate.

**Q4:** *Line 35: As far as I remember does the Dierking paper discuss problems and requirements for retrieving the sea ice surface topography of drifting ice but demonstrates it only for landfast ice.*

**A4:** Yes, Dierking's paper theoretically discussed the impacts of sea-ice drifting velocity on the retrieval of topographic heights and calculated the interferometric sensitivity. However, an example of InSAR retrieval was conducted over landfast sea ice near the coastline of Barrow. We have revised the sentence as:

Notably, the advent of single-pass interferometric SAR (InSAR) sensors, exemplified by TanDEM-X, presents an unprecedented opportunity to generate sea ice DEMs over landfast sea ice (Dierking et al., 2017; Yitayew et al., 2018). For drifting ice, the accuracy of InSAR-derived DEMs can be affected by additional phase shifts induced by ice motion. Dierking et al. (2017) calculated and theoretically discussed the sensitivity of InSAR-derived DEMs concerning ice-drifting velocity, InSAR frequency, and baseline configuration.

**Q5:** *Line 43 and lines 54-55: "Antarctic old ice" – what precisely is "old ice"? The separation between "young ice" and "old ice" based on the criterion of penetration depth (the difference between DMS and SAR elevation) is not suitable, since salinity (as the major factor influencing the μ-wave penetration) is not only linked to ice age but also to other factors (e.g. saline snow crusts at the ice surface, effects of ice flooding). This is also visible in your data, Figs. 13-15. I propose that you instead use the categories "low-penetration condition" and "large-penetration condition".*

**A5:** The "Antarctic old ice" refers to the ice that has a penetration depth (the difference between DMS and SAR elevation) larger than $0.3\,\mathrm{m}$. We agree with the reviewer that the penetration does not simply depend on the age but on the geophysical

conditions of snow and ice. In the revision, we have modified all the "older ice (OI)" and "younger ice (YI)" into the large-penetration condition ice (LPI) and small-penetration condition ice (SPI).

**Q6:** *Lines 59-61: Sentences: "A root-mean-square error (RMSE) of 0.26m between the derived DEM and reference data signifies a precise elevation mapping for both YI and OI. Throughout the paper, "sea ice elevation" is the entire vertical height (including snow depth) above the local sea surface." Actually, 0.26 m (for averages over areas of several meters side length) can locally be a rather high (but mostly acceptable) uncertainty, considering that a large fraction of Antarctic sea ice is first-year with a thickness of around one meter (https://www.climate.gov/news-features/understanding-climate/understanding-climate-antarctic-sea-ice-extent) and correspondingly much less elevation above the water surface. "Precise" means that repeated measurements are close to one another – here the term "accurate" may be more appropriate.*

**A6:** In the Section Introduction, we have revised the sentence as:

A root-mean-square error (RMSE) of $0.26\,\mathrm{m}$ between the derived DEM and reference data indicates an improved accuracy in elevation mapping.

In the Section Conclusion, we have added some texts to discuss the RMSE for both large-penetration condition ice and small-penetration condition ice a bit more:

The uncertainty level is satisfactory for LPI with RMSE of $0.26\,\mathrm{m}$. However, this accuracy is insufficient for thinner ice whose height above sea level is only tens of centimetres or even less. Given that a substantial portion of Antarctic sea ice consists of first-year ice with a thickness of approximately one meter (Scott 2023), achieving precise DEM retrieval over thinner ice remains a challenge. In the future, a potential single-pass InSAR configuration using a higher frequency, such as Ku-band, along with a longer cross-track baseline, would result in a smaller height of ambiguity (HoA) of less than $5\,\mathrm{m}$ (López-Dekker et al., 2011). This setup can enhance InSAR sensitivity and improve the accuracy of total freeboard measurements.

Scott, M.: Understanding climate: Antarctic sea ice extent., NOAA Climate Government, https://www.climate.gov/news-features/ understanding-climate/understanding-climate-antarctic-sea-ice-extent, accessed March 22, 2024., 2023.

López-Dekker, Paco, et al. "TanDEM-X first DEM acquisition: A crossing orbit experiment." IEEE Geoscience and Remote Sensing Letters 8.5 (2011): 943-947.

**Q7:** *Line 87: Here it is ground-range? Is the pixel size of 10 × 10 m used for both the classification process and for elevation retrieval? Should be stated.*

**A7:** Yes, it is ground-range and used for the following sea ice classification and DEM retrieval. We have added a statement:

The multilooking processing was conducted using a $4 \times 12$ window, resulting in a $\sim 10 \times 10\,\mathrm{m}$ pixel spacing in azimuth and ground range. This resolution of $\sim 10 \times 10\,\mathrm{m}$ was subsequently utilized for the sea ice classification and DEM retrieval detailed in Section 3.

**Q8:** *Line 97: The vertical accuracy of the DMS data (line 232) should also be mentioned here. Which reference surface was used for the height values? The local water surface or a reference ellipsoid? In the User Guide by Dotson and Arvesen I found "The IceBridge DMS L3 Photogrammetric DEMs are GeoTIFF imagery, in meters and above the WGS-84 ellipsoid." (page 5). The WGS-84 ellipsoid is usually not at the same level as the local water surface.*

**A8:** We have added the vertical accuracy:

...the OIB aircraft captured optical images (Dominguez, 2010, updated 2018) and generated DEM using photogrammetric techniques at a spatial resolution of approximately $40\,\mathrm{cm} \times 40\,\mathrm{cm}$ with a vertical accuracy of $0.2\,\mathrm{m}$ (Dotson and Arvesen., 2012, updated 2014).

Yes, the height values directly extracted from DMS DEM are above the WGS-84 ellipsoid. In the postprocessing of DMS DEM, we calibrated the values to the local sea level by selecting the water-surface reference from DMS images. For each SAR image, we labeled around ten points as water-surface references according to the DMS images. The average height of the open-water points was subtracted from the origin DMS DEMs to obtain the values relative to the average sea level.

The above processing was described in our previous work (Huang et al., 2021). In the revision, we have added some texts in Section 2.3 for clarification:

Note that DMS DEM gives height values relative to the WGS-84 ellipsoid. To obtain the total freeboard, we calibrated the DMS DEM to the local sea level through a manual process involving the selection of the water surface from DMS images

(Huang et al., 2021). The calibrated DMS DEM, henceforth referred to as DMS DEM for brevity, is utilized as the validation data throughout the paper.

Huang, L., Fischer, G., and Hajnsek, I.: Antarctic snow-covered sea ice topography derivation from TanDEM-X using polarimetric SAR455 interferometry, The Cryosphere, 15, 5323–5344, https://doi.org/10.5194/tc-15-5323-2021, 202

**Q9:** *Lines 115-117: I checked the types of ice charts at the US National Ice Center (https://usicecenter.gov/Products/AntarcHome). I recommend that you provide a link for your reference ("U.S. National Ice Center., 2020") and show the ice chart which you actually used. E.g., I did not find any hint that the ice charts are averages over 7 days, but are produced once a week (https://nsidc.org/sites/default/files/documents/user-guide/g10013-v001-userguide.pdf).*

**A9:** We agree with the reviewer. We have updated the statement:

The U.S. National Ice Center's Antarctic sea ice charts (referred to as Ice Charts hereafter) offer weekly products detailing total sea ice concentration, partial concentration, and stage of development (U.S. National Ice Center., 2022).

We updated the reference with a link:

U.S. National Ice Center.: U.S. National Ice Center Arctic and Antarctic Sea Ice Charts in SIGRID-3 Format, Version 1, https://doi.org/10.7265/4b7s-rn93, 2022.

**Q10:** *Section 2.4: The definition of an "average ice type" does not make sense. With regard to the notation, it is more an "ice condition index". A meaningful comparison between ice type and topography is achieved when the concentration of the respective ice type in your window is sufficiently large, e.g. $>$ 80% or even larger. One has to consider that the topography for one ice type can be highly variable (determined by zones of deformation and their areal fractions relative to the smooth level ice areas). Hence one better concentrates on windows for which one ice type is clearly dominant. In your case that should not be a problem.*

**A10:** We revised the manuscript according to this comment together with the latter one Q21.

We did not establish a strict threshold to select the dominant ice type; instead, the ice concentration percentages for each ice type (MYI, FYI, and TI) from the Ice Charts are displayed in the plot, allowing for a more comprehensive visual comparison with the SAR-derived results.

Note that we have checked carefully that the updated plots do not change any given interpretations or conclusions within the Section Results.

The updated plots are shown below and have been added to the revision:

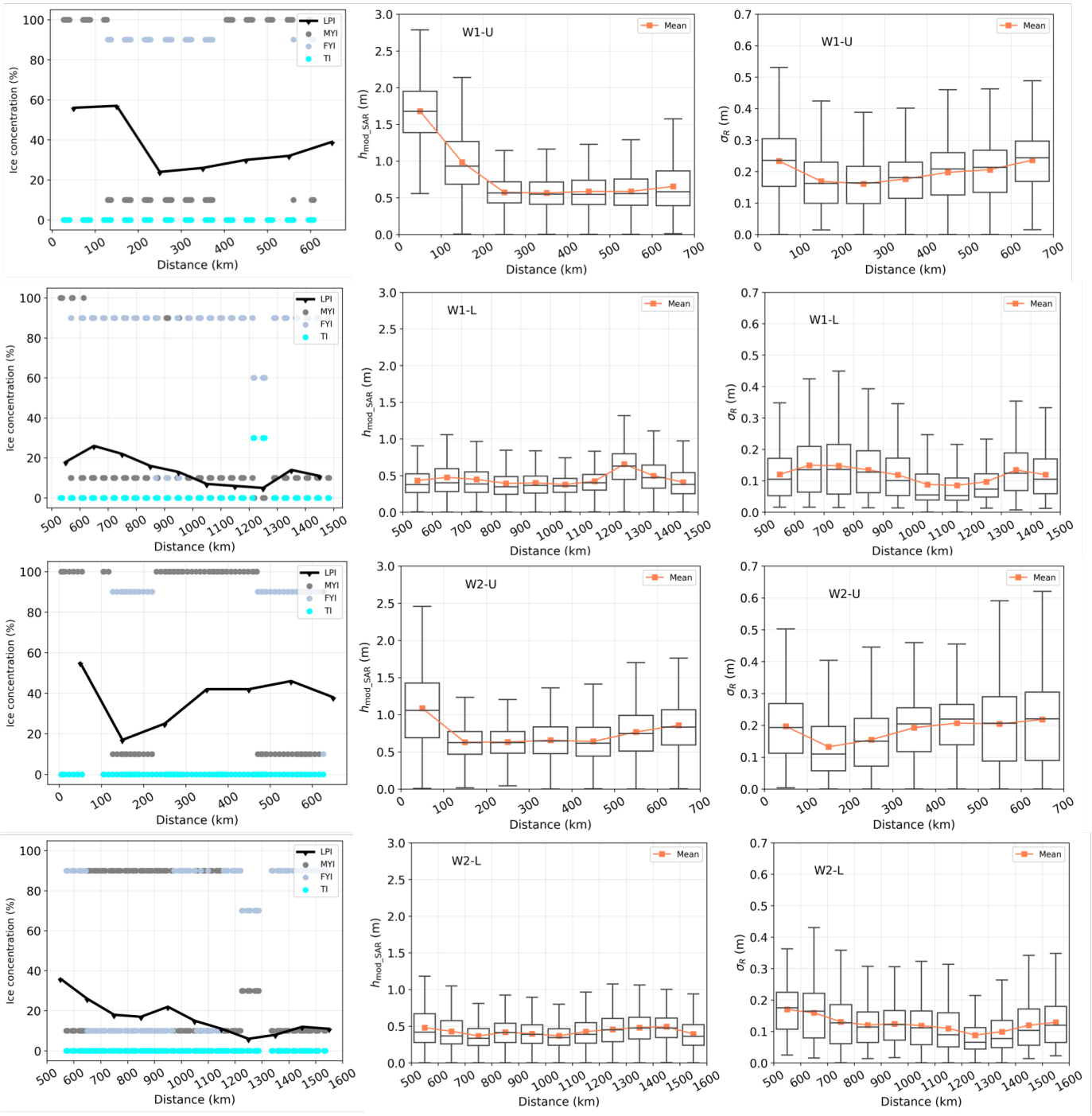


Fig. 1: Sea ice characteristics along the southwards direction along W1 and W2 segments. The blue line in the first column displays the OI percentages derived from SAR images, and the blue dot indicates the ice types obtained from the Ice Charts. The second and third columns plot the elevation ($h_{\mathrm{mod\_SAR}}$) and roughness ($\sigma_R$), respectively. Distance is measured from the northernmost SAR image reference point towards the south. The orange line denotes the average values of $h_{\mathrm{mod_SAR}}$ and $\sigma_R$. The box's upper and lower boundaries represent the first (Q1) and third (Q3) quartiles, while the upper (lower) whisker extends to the last (first) sample outside of Q3 $\pm 1.5\times$(Q3-Q1).

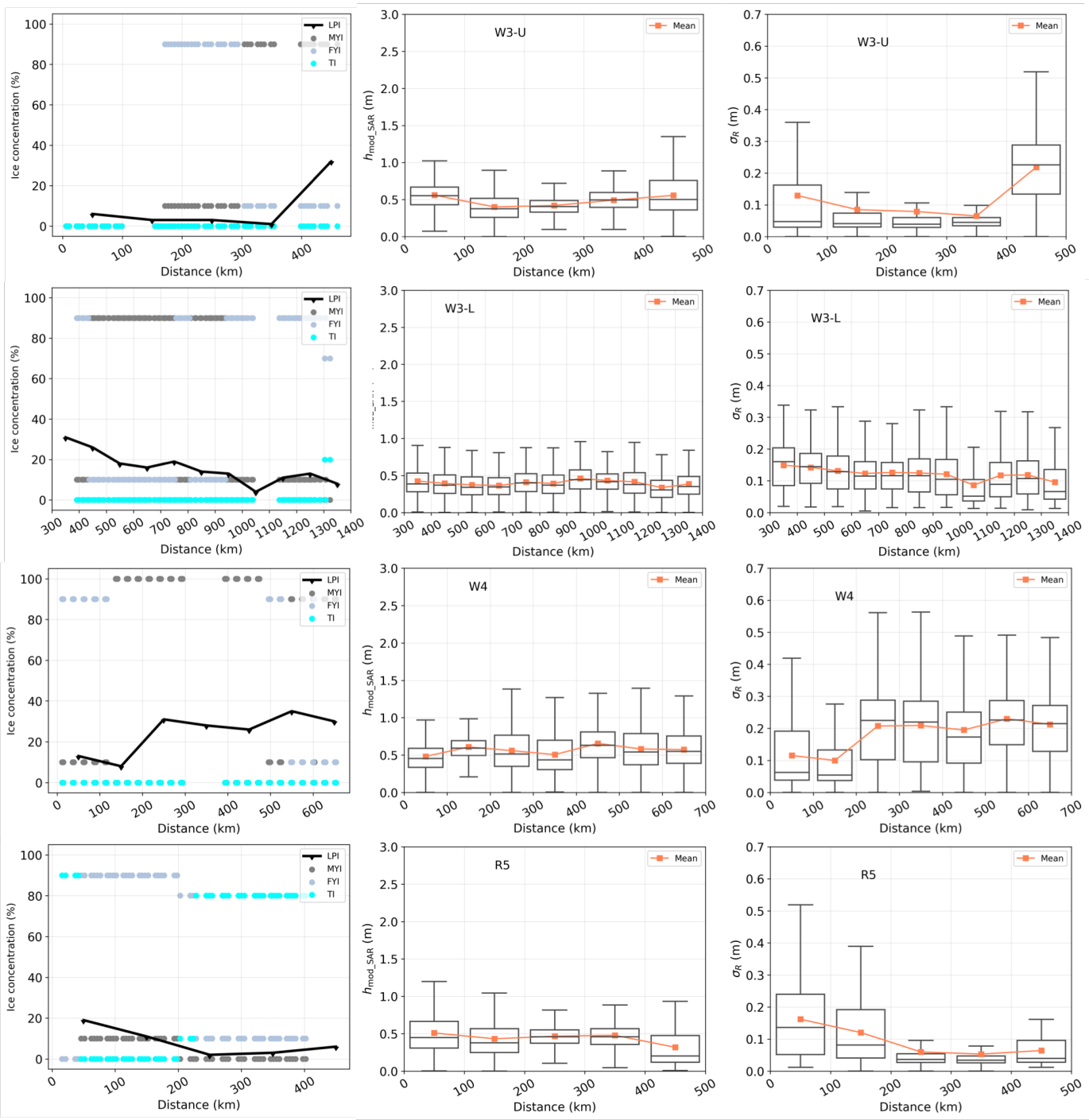


Fig. 2: Sea ice characteristics along the southwards direction along W3, W4, and R5 segments. The blue line in the first column displays the OI percentages derived from SAR images, and the blue dot indicates the ice types obtained from the Ice Charts. The second and third columns plot the elevation ($h_{\mathrm{mod\_SAR}}$) and roughness ($\sigma_R$), respectively.

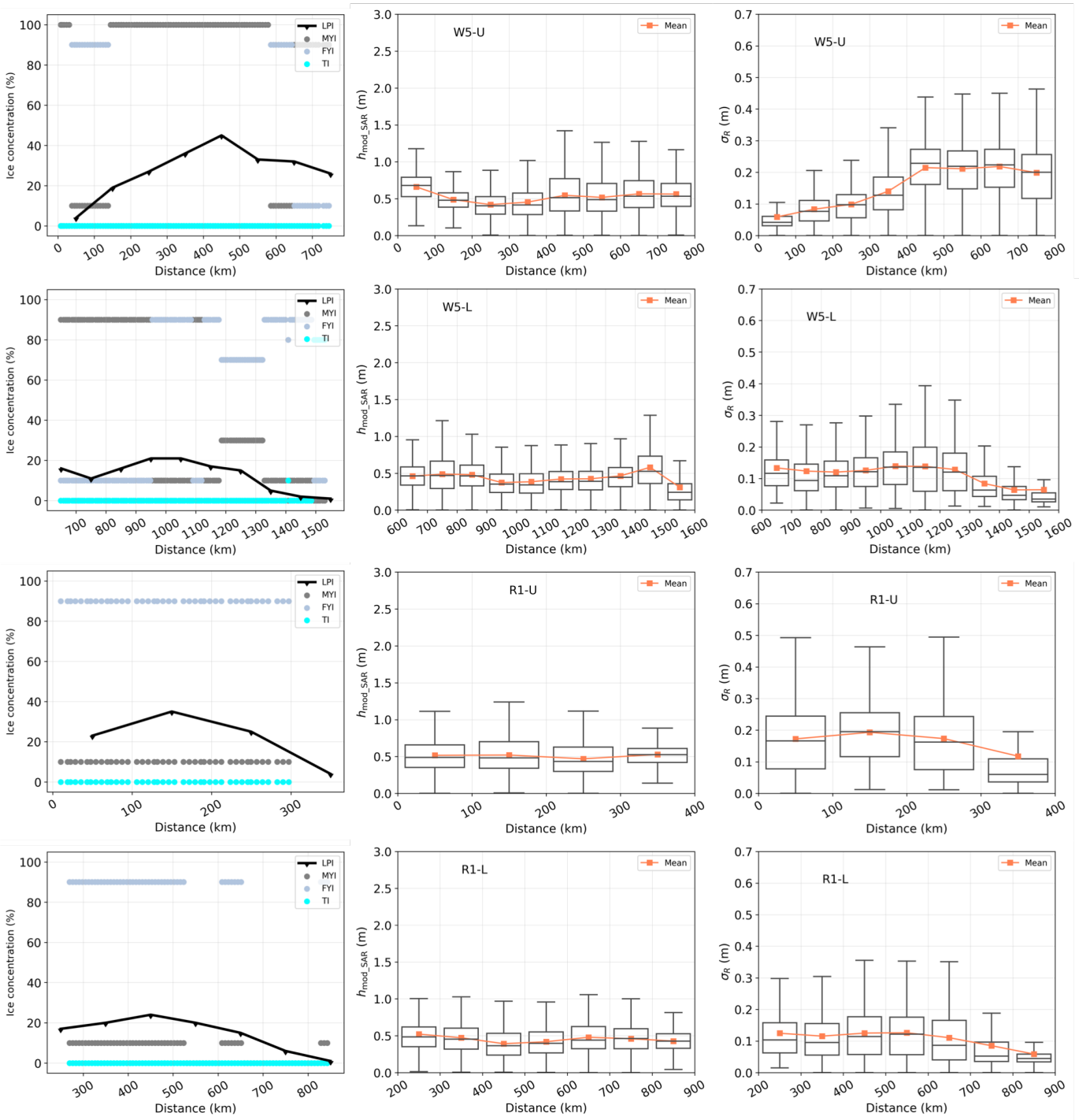


Fig. 3: Sea ice characteristics along the southwards direction along W5 and R1 segments. The blue line in the first column displays the OI percentages derived from SAR images, and the blue dot indicates the ice types obtained from the Ice Charts. The second and third columns plot the elevation ($h_{\mathrm{mod\_SAR}}$) and roughness ($\sigma_R$), respectively.

**Q11:** *Line 148: what are "Pauli-1" and "Pauli-2"-polarizations? Do you refer to the Pauli-representation? Then Pauli-1 is the first and Pauli-2 the second component of the Pauli decomposition which relates surface and volume scattering?*

**A11:** The Pauli decomposition leads to the generation of the "Pauli feature vector" as:

$k = \frac{1}{\sqrt{2}}[s_{\mathrm{HH}} + s_{\mathrm{VV}}, s_{\mathrm{HH}} - s_{\mathrm{VV}}, 2s_{\mathrm{HV}}]$

where $s_{\mathrm{HH}}$, $s_{\mathrm{VV}}$ and $s_{\mathrm{HV}}$ are the complex backscattering signal in HH, VV, and HV polarizations, respectively. This representation allows separating odd, even and the 45° tilted bounce components.

Pauli-1 = $s_{\mathrm{HH}} + s_{\mathrm{VV}}$ represents odd bounce, usually the surface scattering. Pauli-2 = $s_{\mathrm{HH}} - s_{\mathrm{VV}}$ represents even bounce. In our SAR data, we do not have HV polarizations therefore only Pauli-1 and Pauli-2 were calculated and used.

In the revision, we have updated the Eq.6 as

Similarly, we can obtain the Pauli-polarization ratio ($R_{\mathrm{pauli}}$) by

$$R_{\mathrm{Pauli}} = \frac{\sigma_{\mathrm{P1}}}{\sigma_{\mathrm{P2}}} = \frac{|s_{\mathrm{HH}} + s_{\mathrm{VV}}|^2}{|s_{\mathrm{HH}} - s_{\mathrm{VV}}|^2} \tag{1}$$

where $\sigma_{\mathrm{P1}}$ and $\sigma_{\mathrm{P2}}$ are denoised SAR backscattering intensity in Pauli-1 and Pauli-2 polarizations in linear scale, respectively. $s_{\mathrm{HH}}$ and $s_{\mathrm{VV}}$ are single-look complex images in dual-pol channels, respectively.

**Q12:** *Lines 166 – 172: see comment (4) above. There is also a misprint on line 172, it should read "hpene >=0.3 m are OI". Was there a special criterion for selecting a threshold of 0.3 m for separating YI and OI?*

**A12:** We have corrected the statement:

$h_{\mathrm{pene}} \geq 0.3\,\mathrm{m}$ are OI

Hallikainen and Winebrenner (1992), in Figure 3-8, suggested that the radar penetration depth of sea ice over multiyear ice ranges from 0.3 to 1 meter at X-band (9.65 GHz - 10 GHz), depending on temperature. Dierking et al. (2017) suggested that ice blocks within ridges often undergo desalination, leading to a greater effective penetration depth within the ridged ice compared to adjacent level ice. This difference in penetration depth can reduce the apparent ridge height relative to the level ice surface as observed in the interferogram. Given that the study area is covered by snow and deformed ice such as ridges, we have selected a penetration depth of 0.3 meters as a threshold for distinguishing between low-penetration and high-penetration ice conditions.

We have added the above texts in Section 3.1 in the revision:

Note that the sea ice penetration depth over multiyear ice is suggested to be $0.3 - 1\,\mathrm{m}$ at the X-band, which varies with temperature (Hallikainen and Winebrenner, 1992). Desalination within ice ridges increases the effective penetration depth compared to level ice (Dierking et al., 2017). Considering these findings and given the study area's snow cover and the presence of deformed ice such as ridges, we chose a penetration depth of $0.3\,\mathrm{m}$ as the threshold for distinguishing the two ice types (i.e., SPI and LPI).

Hallikainen, M. and Winebrenner, D. P.: The physical basis for sea ice remote sensing, Microwave remote sensing of sea ice, 68, 29–46, https://doi.org/10.1029/GM068p0029, 1992

Dierking, W., Lang, O., and Busche, T.: Sea ice local surface topography from single-pass satellite InSAR measurements: a feasibility study, The Cryosphere, 11, 1967–1985, https://doi.org/10.5194/tc-11-1967-2017, 2017.

**Q13:** *Lines 185 – 186: The question is how your "YI" class is related to the ice types listed in Table 2. The WMO-category defines young ice as ice between 10 cm and 30 cm in thickness, as correctly listed in your table. It can be assumed that a penetration depth up to 0.3 m (your "YI") covers the categories "Thin Ice" and "First-Year Ice". The "old ice" with a penetration depth >= 0.3 m cover the thicker FY ice and MY ice. Conclusion is that you should not use the notation YI for penetration depths < 0.3m, see comment 4 above. Check also notations used in section "Conclusions".*

**A13:** We agree with the reviewer. As suggested in A5, we have replaced the "YI" and "OI" terms with the small-penetration condition ice (SPI) and large-penetration condition ice (LPI) throughout the manuscript.

**Q14:** *Figure 6 and Section 2.5: How do you relate hInSAR to the local water surface? Or in other words: which reference surface do you actually use when calculating hInSAR? I suppose that in the initial InSAR processing it is not the local water surface but also the WGS84-elliposid?*

**A14:** The initial height $h_{\mathrm{InSAR\_ini}}$ generated from InSAR processing was referenced to the WGS84 ellipsoid. In theory, we could identify the pixels of the water area and calibrate the InSAR height relative to the water surface by $h_{\mathrm{InSAR}} = h_{\mathrm{InSAR\_ini}} - h_{\mathrm{InSAR\_water}}$. However, due to the low InSAR coherence (less than 0.3) in water areas, these water pixels were masked out as the $h_{\mathrm{InSAR\_water}}$ are inaccurate and can not be used for analyses. Hence, instead of identifying water pixels, we selected smooth and new ice regions, assuming they are thin enough and their elevation (i.e., radar freeboard) is negligible and approximately equal to the water surface. These areas typically exhibit very low SAR backscattering intensity values in both HH and VV polarizations, ranging from -19dB to -18dB, slightly above the noise level of TanDEM-X (-19dB). By generating

a histogram of $h_{\mathrm{InSAR\_ini}}$ values for the thin-ice pixels, we determined the 3rd percentile of the height of these thin-ice pixels to be the local water surface elevation ($\approx h_{\mathrm{InSAR\_water}}$). The threshold value, i.e., the 3rd percentile, is chosen by conducting the aforementioned method over the four SAR scenarios overlaid with DMS DEM (refer to Fig. 2 in the manuscript). When choosing the 3rd percentile as the water surface level, we verify that the calibrated $h_{\mathrm{InSAR}}$ matches the $h_{\mathrm{DMS}}$ at the same level, confirming the validity of the threshold value.

Note that we performed the aforementioned processing for each SAR scene, covering an area of $50 \times 19\,\mathrm{km}$. This approach resulted in one value representing the local water surface for each SAR scene. This method may introduce inaccuracies due to the centimeters level of the radar freeboard of the selected thin and new ice, as well as the fluctuating water surface within each SAR scenario. In the revision, we have included the above text in a new Section Discussion.

**Q15:** *Section 3.2. Here, many things are unclear to me. In summary, I recommend to rewrite this section for the sake of clarity. Single issues: (a) what is the exact definition of m, does it refer to thickness of layer 1 and layer 2? (b) Is hmod the surface elevation above the water surface (or reference ellipsoid)? (c) Which AMSR Level 3 data did you use for retrieving the snow depth over your test sites? How large is the uncertainty of those snow depth values? (d) line 202: "$\phi_{DMS}$ can be transformed into $\phi_{DMS}$ by Eq. (3)" : equation 3 describes the relation between hInSAR and $\phi_\gamma$. I wonder whether this equation can be simply applied using hDMS to derive $\phi_{DMS}$ because for the DMS data there is no height of ambiguity. Is $\phi_{DMS}$ assumed to be the phase at the snow-air interface, hence $\phi_{DMS} = \phi_0$? (e) From equation 8, you obtain m and hv, according to the given definition and Fig. 6 hv is ice thickness which could be mentioned. (f) Why is the second step needed, namely to combine the SAR features with m and hv to obtain modified values m' and hv' ? With the classified images (your maps of ice types), one can directly link the m and hv values from the first step in Fig. 7 with the corresponding ice classification map. The second step is not needed.*

**A15:** (a) In previous study, we proposed a layer-to-layer scattering ratio ($m$) (Huang et al. 2021), inspirated from the concept of the layer-to-volume scattering ratio utilized in ice sheeting (Fischer et al., 2018).

The layer-to-layer scattering ratio ($m$) refers to the backscattering power ratio between the top and bottom layer:

$$m = \frac{\sigma_{bottom}(\vec{\omega})}{\sigma_{top}(\vec{\omega})}$$

where $\sigma_{top}\vec{\omega})$ and $\sigma_{bottom}(\vec{\omega})$ denotes the backscattering power from the top and bottom interface, respectively, for a given polarization channel $\vec{\omega}$.

$m$ potentially reveals the relative importance of scattering from these interfaces, depending on factors like interface roughness, dielectric constant, and radar polarization. A larger value of $m$ signifies that surface scattering from the bottom layer predominates, while a smaller $m$ indicates that surface scattering from the top layer is more significant.

(b) $h_{\mathrm{mod}}$ refers to the elevation of the snow-air interface above the water surface.

(c) We used the AMSR-E/AMSR2 Unified L3 Daily 12.5 km Brightness Temperatures, Sea Ice Concentration, Motion & Snow Depth Polar Grids, Version 1 dataset (https://doi.org/10.5067/RA1MIJOYPK3P) for our study. The provided snow depth over sea ice represents a five-day running average. Due to the limited spatial and temporal resolution in the snow depth data, we assumed a constant value of snow depth across one SAR image. For each SAR acquisition, covering a spatial extent of $50 \times 19\,\mathrm{km}$, we computed the mean snow depth and utilized it as input parameter $z_1$ in the TLPV model. In our previous study (Huang et al., 2021), we evaluated the TLPV model's performance concerning variations in snow depth. Our findings indicated a mean discrepancy of $0.31\,\mathrm{m}$ in the derived total freeboard due to snow depth fluctuations ranging from $0.05$ to $0.75\,\mathrm{m}$, which covers the major ($> 95\%$) snow depth range in the Weddell Sea during Webster et al. (2018). In future investigations, it would be promising to adapt our proposed total freeboard retrieval method to test sites that coincide with available high-resolution snow depth measurements.

(d) For InSAR, there is a general equation accounting for the relation between the interferometric phase ($\phi$) and height ($h$)

$$h = h_a \frac{\phi}{2\pi}$$

where $h_a$ is the height of ambiguity determined by the specific InSAR configuration such as the radar wavelength, orbit height, incidence angle, and baseline. In instances where we have an external DEM, such as from photogrammetry or lidar, we can also simulate the interferometric phase ($\phi_{\mathrm{DMS}}$) from the height ($h_{\mathrm{DMS}}$) using the same equation tailored to a specific InSAR

configuration giving specific $h_a$.

Yes, $\phi_{\mathrm{DMS}} = \phi_0$.

(e) $hv = z_1 - z_2$ represents the depth between the top ($z_1$) and bottom ($z_2$) interfaces, which contribute to surface scattering effects. However, it's important to note that the bottom layer is not always at the ice-water interface. In some cases, a lower basal sea ice layer can exist, as discussed in Nghiem et al. (2022), which induces strong surface scattering from the ice-basal layer interface. This basal saline layer contains brine inclusions with higher salinity, transitioning toward the ice-seawater interface, as observed in the Western Weddell Sea (Tison et al., 2008). The salinity in this basal layer can be attributed to past flooding events on younger, thinner ice that eventually becomes older and thicker. Furthermore, brines in the upper ice volume above the sea level drain down, further salinating the lower basal layer (Nghiem et al., 2022). Therefore, in scenarios where a high-salinity basal layer is present, $hv$ may not be equivalent to the ice thickness.

Nghiem, S. V., Huang, L., and Hajnsek, I.: Theory of radar polarimetric interferometry and its application to the retrieval of sea ice elevation in the Western Weddell Sea, Antarctic, Earth Space Sci., 9, e2021EA002 191, https://doi.org/10.1029/2021EA002191, 2022.

Tison, J.-L., Worby, A., Delille, B., Brabant, F., Papadimitriou, S., Thomas, D., & Haas, C. Temporal evolution of decaying summer first-year sea ice in the Western Weddell Sea, Antarctica. Deep-Sea Research Part II: Topical Studies in Oceanography, 55(8–9), 975–987. https://doi.org/10.1016/j.dsr2.2007.12.021, 2008

(f) First, $m$ and $h_v$ were calculated by inverting Eq.(8) using $\phi_{\mathrm{DMS}}$ ($= \phi_0$) as input. In the subsequent step, assuming $m$ and $h_v$ from the first step as true values, we established an empirical relation (RF regression) between SAR features and $m$ and $h_v$, enabling estimation of these parameters solely using SAR data, denoted as $\hat{m}$ and $\hat{h}_v$. For the SAR scene without overlapped DMS measurements, the $\hat{m}$ and $\hat{h}_v$ are input into Eq.(8) to generate $h_{\mathrm{mod}}$, which is the total freeboard for the large-penetration condition ice.

In the revision, we have added the above texts and rewritten the section for clarity. We have also updated the method flowchart for clarity, see below:

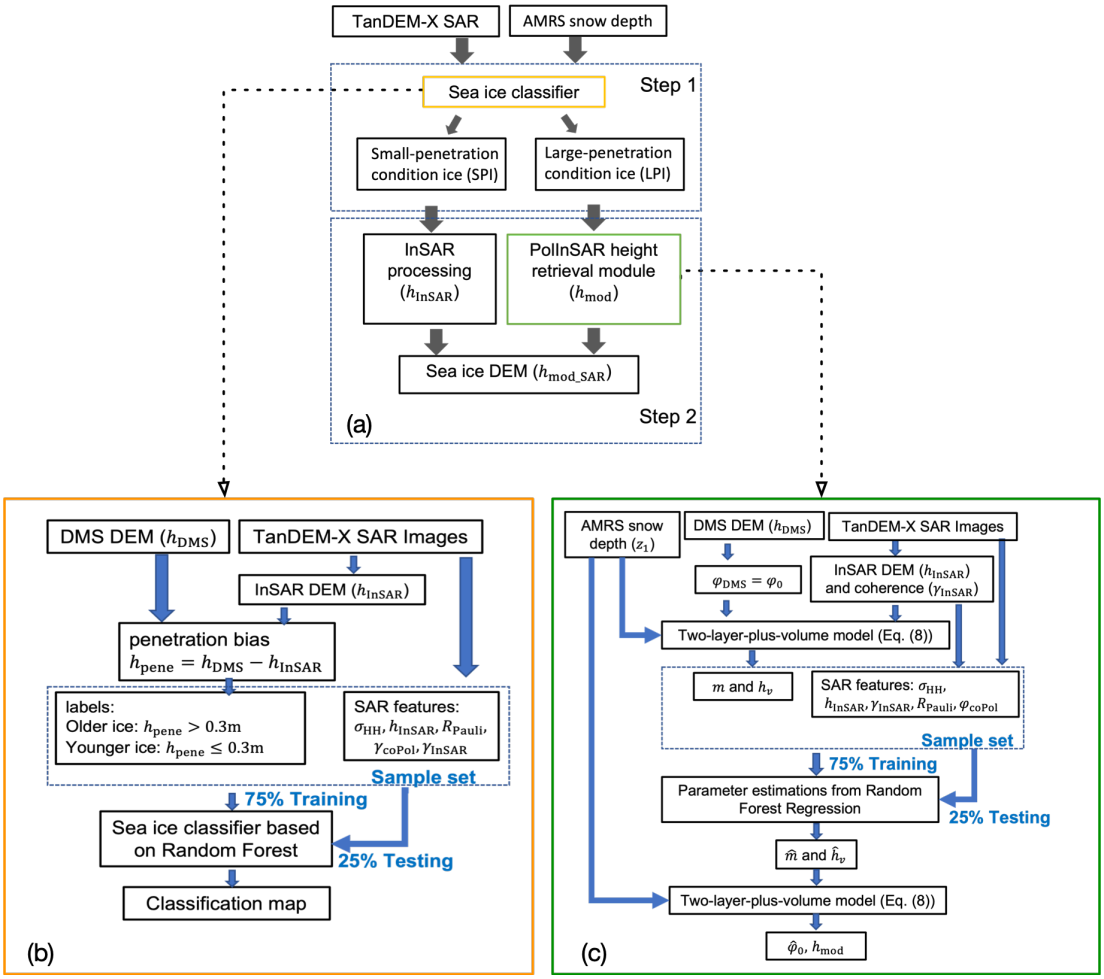


Fig. 4: (a) The proposed two-step approach for sea ice DEM retrieval. (b) The details (training and validation) of the sea ice classifier and (c) the PolInSAR height retrieval module.

**Q16:** *Fig 9: the right-most color bar is "E", is this the DEM given in meters?*

**A16:** The DEM is given in meters. We apology for the confusion. It is "m" (stands for meters) but printed vertically. We have updated the colorbar label to "meter".

**Q17:** *Figure 11: What is the explanation for the data gaps in the second profile from the top?*

**A17:** The data gaps are the water areas and segments that were excluded due to inaccurate data co-registration. During InSAR processing, pixels with InSAR coherence below 0.3 were masked out. Additionally, during data co-registration between DMS and SAR, segments lacking distinctive sea ice features in optical and SAR images, and hence, unable to ensure co-registration quality, were eliminated.

We have added explanations in Section 2.3:

Note that the segments lacking distinctive sea ice features in optical and SAR images were eliminated to ensure co-registration quality.

We also added an explanation in the caption of Fig 11:

Figure 11. Comparison between the elevation profiles ($h_{\mathrm{mod\_SAR}}$) from the proposed method and the DMS DEM ($h_{\mathrm{DMS}}$) along the dotted line (from A to B) over Scene No.1-4 in Fig.9(c). The data gaps are the water areas and segments that were excluded due to inaccurate data co-registration.

**Q18:** *Results shown in Figs. 9, 10, 11: hmodSAR is elevation = total freeboard relative to the water surface (or reference ellipsoid), retrieved from pixels of 10 × 10 m in size?*

**A18:** Yes, $h_{\mathrm{modSAR}}$ are total freeboard relative to the water surface retrieved from $10 \times 10\,\mathrm{m}$ pixel size. In the revision, we have added the texts at the second paragraph in Section 4.1:

Note that $h_{\mathrm{modSAR}}$ represents total freeboard relative to the water surface retrieved from the pixel at $10 \times 10\,\mathrm{m}$ spacing size.

**Q19:** *Again Figs. 9, 10, 11: For "old ice", height values = total freeboard of even larger than 3 m are measured. Intuitively, this seems to be not very realistic, although DMS and SAR values match. Is there any information available about the area regarding ice and snow conditions which seems to be special when comparing to the results of the other profiles shown in Figs. 13-15 which reveal smaller heights? If you used the WGS84 ellipsoid as reference: Is the difference between reference ellipsoid and mean sea level larger close to the Antarctic Peninsula? Perhaps also icebergs biased the measurements?*

**A19:** The four scenarios depicted in Figures 9, 10, and 11 in the manuscript are located near the Eastern Antarctic Peninsula (see Fig 2 in the manuscript for the geolocation). Notably, we observed considerable deformation and prominent ridges in the sea ice from the DMS photo. While, upon thorough examination of DMS photos across the four scenes, no icebergs were identified. Therefore, we think it is the deformed ice and ridges contribute to the high total freeboard values.

Here, we show a DMS photograph captured a sub-region within Scene No.1, see Fig. 5(a) below. In Fig. 5(b), we used the DMS DEM derived from this photograph, annotated specific sea ice features, and extracted corresponding elevation values.

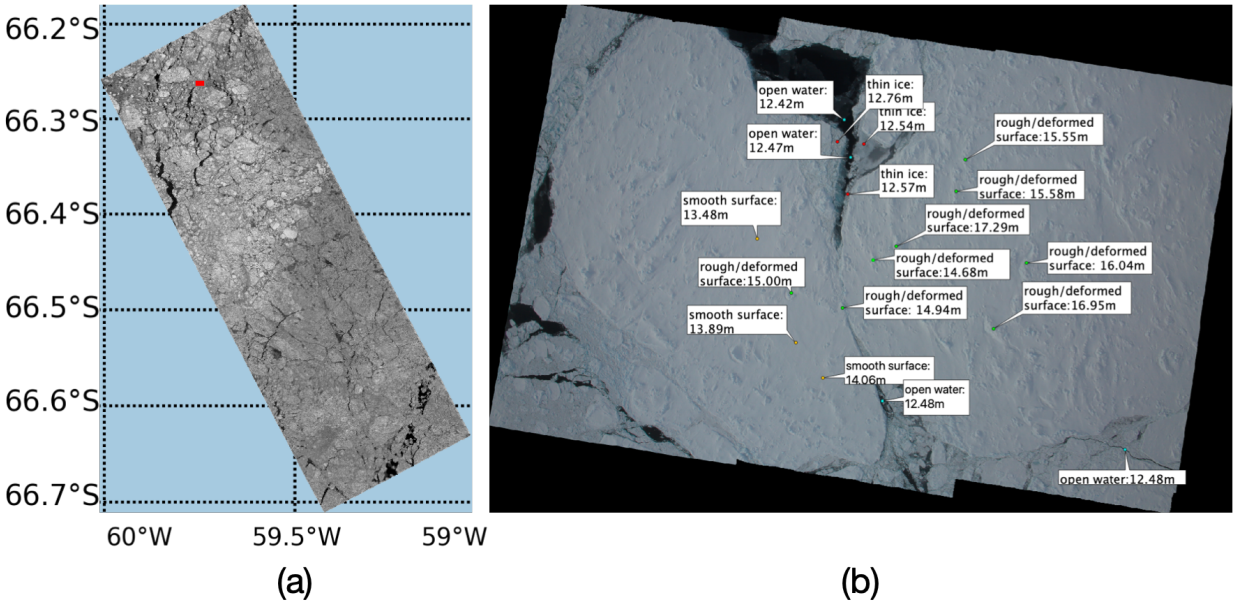


Fig. 5: The red rectangle indicates the selected sub-region overlapped by DMS measurements. (b) The optical photo alongside elevations derived from the DMS DEM within the selected sub-region. The elevation values are referenced to the WGS84 Ellipsoid.

The elevation values in Fig. 1(b) are referenced to the WGS84 Ellipsoid, representing the original values obtained from the DMS DEM products. The water surface ranges between 12.4-12.5m, while the thin ice adjacent to the water ranges from 12.5-13.0m, indicating a relative elevation of 10-50 centimeters compared to the water surface. On the ice floes, the smooth surfaces measure around 13.0-14.0m, representing an elevation of 0.5-1.5m above the water surface. The rough surfaces, including deformed ice and ridges, exhibit elevations ranging from 14.5-17m, with corresponding relative elevations to the water surface exceeding 3m.

**Q20:** *Figure 12: The color bars show values of hmodSAR down-sampled to a resolution of 500 m?*

**A20:** Yes, the results in Sections 4.2, 4.3, and 4.4 (including Fig.12-16) are all based on the $h_{\mathrm{modSAR}}$ down-sampled to $500\,\mathrm{m}$. We stated this in the beginning of Section 4.2. In the revision, we have added the statement in the caption of Fig.12:

$h_{\mathrm{mod\_SAR}}$ was downsampled to $500\,\mathrm{m}$ pixel size.

**Q21:** *Figures 13,14,15, left column: The percentage of "OI" refers to the large-penetration-depth category. It would be much easier to discuss the relationship between the OI and real ice types when concentrations of MY, FY, and TI are shown*

*instead of an index related to the "average ice type". Lines 241-243: In Fig. 13, the percentage of OI is only 58% for distances between 0 and 160 m, but the ice type in the ice chart seems to be almost 100% MYI ice since the "average ice type" value is close to 3. In the range between approximately 300 and 600 km, MYI is also close to 100% concentration, but the percentage of OI is down to 20-25%. (Note that according to section 2.4, the indices for TI, FYI, and MYI should be 0,1,2, respectively, and not 1,2,3) This demonstrates that the penetration depth is not directly linked to the ice types shown in the ice chart.*

**A21:** We have renamed the "OI" as large-penetration condition ice (LPI) in the revision. We have updated the results by showing the ice types with concentrations, see **A10**.

The ice concentration values for MYI from Ice Charts and the LPI percentage from SAR are not necessarily identical, as they are classified by different criteria. Nevertheless, our study observed and discussed a similar trend between the dominant ice types and ice concentrations from the Ice Charts and the LPI percentage from SAR. We have replaced lines 241-248 in the previous with the texts below:

The overall trend of estimated OI percentages correlates well with dominant ice types and ice contractions from the Ice Charts across most segments (W1-U, W1-L, W2-U, W4, W5-U, W5-L, and R5). Specifically, W1-U and W1-L are explained as two examples. W1-U from 0-120km is covered by 100% MYI, where the LPI percentage reaches its highest value (58%). As the dominant ice transitions from MYI to FYI from 120-400km, the LPI percentage decreases accordingly. For W1-L, where the distance between 500-600km is covered by 100% MYI, and the LPI percentage peaks before decreasing after 650km distance as FYI becomes dominant. The lowest LPI percentage is found around 1200km, consistent with the occurrence of TI at this distance.

The observed similar trend can be explained by the general assumption that MYI is thicker and less saline, allowing for deeper radar penetration compared to FYI and TI. However, penetration depth is influenced by various factors not only ice age, but also ice salinity, snow condition, flooding effects, and temperature. This explains the discrepancies for other segments (W2-L, W3-U, W3-L, R1-U, R1-L). Furthermore, discrepancies can also be attributed to differences in spatial resolution and temporal gaps between Ice Charts and SAR imagery, considering the dynamic nature of sea ice.

It is essential to clarify that we utilized Ice Charts data as an external information source to interpret the classification results and spatial variation of topography. However, we did not use Ice Charts to quantitatively validate the proposed method. For validation purposes, we conducted pixel-by-pixel comparisons using co-registered DMS data.

**Q22:** *Line 253-261: Referring to the statement: "In general, the region with thicker ice (e.g., MYI) is anticipated to display higher elevation or larger roughness compared to the area with thinner ice, such as FYI and TI": Locally, rough FYI may reveal a larger roughness than smooth level MYI, and it may reveal a higher elevation when covered by a very thick snow cover. This may also explain discrepancies.*

**A22:** Agree. In the revision, we have added the explanation for the discrepancies as suggested:

These discrepancies may arise due to the local cases where rough FYI exhibits greater roughness than smooth level MYI. FYI may also show higher elevations when covered by very thick snow.

**Q23:** *Line 262: "sea ice . . . exhibits. . . highest elevation". You should again clearly state that the values of elevation are total freeboard, i.e. also include the snow layer.*

**A23:** We agree. In the revision, we have replaced "elevation" with "total freeboard" throughout the manuscript.

**Q24:** *Line 265: Figs. 6g-l in the paper by Wang et al (2020) are indeed well suited for comparing with your results. The values they show (Fig. 6l for 2017), however, have only a narrow peak at 1.5 to 2.5 m, otherwise values are lower. Figs 6g-l should also be mentioned with regard to your Figs 13-15, considering window sizes for averaging the elevation.*

**A24:** Upon thorough examination of Wang et al.'s work (2020), we were unable to find the resolution (window size) they used for plotting Fig. 6l. However, based on their mention of a $20\,\mathrm{km}$ width track, we estimate that each dot corresponds to a window size larger than $20\,\mathrm{km}$, significantly exceeding the $500 \times 500\,\mathrm{m}$ window size we utilized. Unfortunately, Wang et al. did not provide the processed data used in Fig. 6l in the supplements, preventing a quantitative comparison with our results. Therefore, we conducted a visual comparison based on geolocation, comparing Fig. 6l in Wang et al. (2020) with the four segments (W2-U, W2-L, W3-U, and W3-L) in our study, as shown in Fig. 13 and 14 in the manuscript.

We have included Fig. 6l below (as shown in Fig. 6), and we define the two tracks in Fig.6l as Track-W and Track-E. The region with latitude $< 70°\mathrm{S}$ ($> 70°\mathrm{S}$) is referred to as the northern (southern) track.

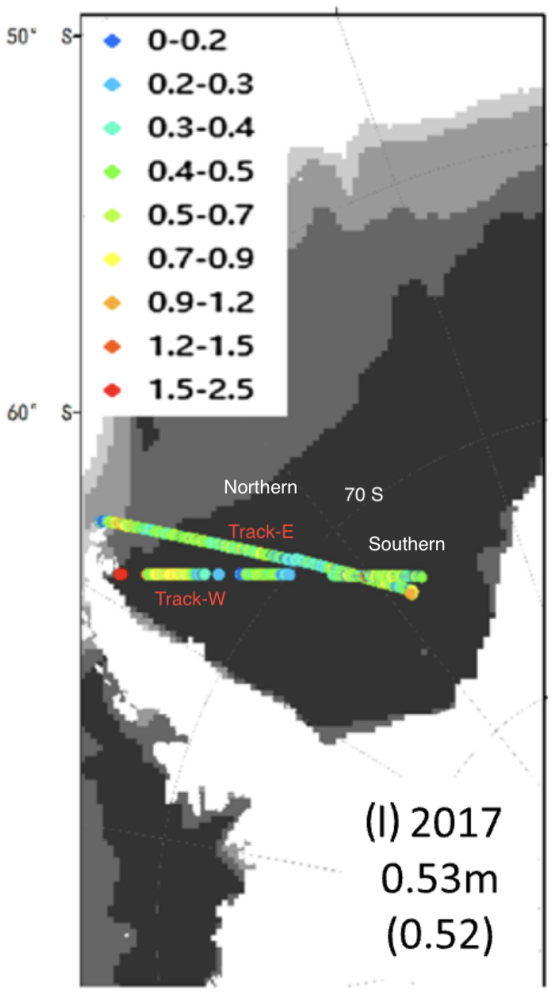


Fig. 6: The total freeboard from the paper by Wang et al., 2020 (Fig.6l). We labeled the two tracks Track-W and Track-E. The region with latitude $< 70°$S ($> 70°$S) is referred to as the northern (southern) track.

The Northern and Southern Track-W segments are partially overlaid with W2-U and W2-L, respectively. In our study, the total freeboard of W2-U and W2-L are shown in the third and fourth rows (medium column) in Fig. 13 (in the manuscript). Our result shows that the total freeboard reaches a mean value of $\sim 1\,\mathrm{m}$ and 75% percentile value of $\sim 1.5\,\mathrm{m}$ within the first $100\,\mathrm{km}$, which agrees with the red dot in Fig.6l Track-W. Then, the total freeboard goes down to a mean value as $\sim 0.7\,\mathrm{m}$ and 75% percentile value of $\sim 0.75\,\mathrm{m}$ from $100 - 200\,\mathrm{m}$. Although there is a data gap in the Fig.6l (Wang's paper), we can see that the color of dots changes from red to yellow, which is consistent with the decreasing trend of the total freeboard within $300\,\mathrm{km}$ from our results. For W2-L, the total freeboard from results are around at the mean values of $0.5\,\mathrm{m}$, agree with a mix of green and yellow dots ($0.5 - 0.9\,\mathrm{m}$) in the Southern Track-W in Fig.6l (Wang's paper).

Note that the OIB ATM data used for Fig.6l was acquired on 14th and 22rd November 2017, while the SAR images in our study were acquired on 30th and 25th October 2017 for W2-U and W2-L. The sea ice drift or potential melting could induce slight differences in our results and Wang's results.

The W3-U and W3-L can be compared with Northern and Southern Track-E, respectively. From Fig. 6l, a mix of yellow and green dots in the northern Track-E represent the total freeboard $0.5 - 1.2\,\mathrm{m}$ total freeboard, which agrees well with our result in W3-U, see the first row in Fig.14 (in the manuscript). At around $70°$S degree, the dots transit to cyan and blue, representing the total freeboard of $0.2 - 0.7\,\mathrm{m}$, which is consistent with the W3-L in Fig.14 (in the manuscript). The slight difference can be attributed to the temporal difference of SAR images used in our study. Specifically, the image for W3-L was acquired on October 26, 2017, while the Track-E image was acquired on November 22, 2017

We have added the above analyses in the revision Sections 4.2 and 4.3.

**Q25:** *Line 283: ice type "MTI"? I think it should be MYI.*

**A25:** Corrected.

**Q26:** *Line 294-295: Sentence: "The variation of the roughness along the R1 segment also highlights the importance of combining topographic mapping with ice category mapping to comprehensively characterize sea ice features." Since there is no direct relationship between ice type and topography data, it is not per se "important" to combine both, but can be useful in certain cases, e.g. for operational ice charting. Since the edges of ice floes with open water between the floes contribute to the ice roughness, ice concentration may also be a useful parameter to be combined with ice topography in some cases.*

**A26:** We agree with the reviewer. We have modified the statement in the revision:

The variation of the roughness along the R1 segment suggests that ice topography provides add-on information that can be useful to be integrated into the operational ice charting. Furthermore, Since the edges of ice floes with open water between the floes can also contribute to the ice roughness, combining ice topography with ice concentration can help characterize the sea ice cover more comprehensively.

**Q27:** *A point of my interest: For radar applications, it would also be useful to show how large deviations between DMS and SAR values (= your penetration depth) can be, and where this occurs (spatial distribution along your tracks).*

**A27:** This is a super interesting point. Considering the studied area is mainly covered by snow, we believe the penetration largely depends on the local snow conditions and snow spatial distributions. Unfortunately, our current dataset does not have in-situ measurements of snow properties, so we cannot investigate the deviation with the snow parameters. In the future, it would be interesting to propose/conduct fieldwork that includes TanDEM-X acquisitions, lidar measurement, and in-situ snow measurements and analyze the relation between the radar freeboard and total freeboard at varying snow depths.

We have added texts in the Section Conclusion as:

The spatial distribution of penetration depth (total freeboard minus radar freeboard) can be an interesting topic for future research. In snow-covered sea ice, penetration is significantly influenced by local snow conditions. Hence, conducting a coordinated campaign encompassing TanDEM-X acquisitions, lidar measurements, and in-situ snow assessments holds great promise for analyzing the relation between radar freeboard and total freeboard across different snow depths.

Again, we sincerely thank the editor and reviewers for helping us improving the manuscript.